POLARIMETRIC RADAR RAINFALL ESTIMATION IN COMPLEX OROGRAPHY SCENARIOS

19B.3 Gianfranco Vulpiani[1], Mario Montopoli[2,3], Pietro Giordano[1], Antonio Gioia[1], Luca Delli Passeri[1] and Frank S. Marzano[3,4]

[1] Department of Civil Protection, Prime Ministry, Rome, Italy
[2] Department of Electrical Engineering, University of L'Aquila, L'Aquila, Italy
[3] CETEMPS, Center of Excellence, University of L'Aquila, L'Aquila, Italy
[4] Department of Electronic Engineering, Sapienza University of Rome, Rome, Italy

1. INTRODUCTION

Radar rainfall estimation is a complex process dealing with several error sources, some of them being related to the environmental context.

At S band and in relatively flat terrain conditions, dual-polarization has been already proven either to increase the data quality or to improve the rainfall estimate (Ryzhkov et al. 2005a,b; Giangrande and Ryzhkov 2008; Vulpiani et al. 2009).

However, most of the European operational weather radar operates at C band, several of them in mountainous areas. In such circumstances, a part from path attenuation that might be severe at C band, the quality of the retrieved radar products is further conditioned by the presence of topographic obstacles. Indeed, together with the enhancement of ground-clutter effects, the major limitation is represented by partial or total beam blocking caused by natural obstructions.

The first investigations concerning topographical effects on polarimetric rainfall measurements have been accomplished by Zrnić and Ryzhkov (1996) and Vivekanandan et al. (1999) using S-band radar observations of single flash flood events. Friedrich et al. (2007) have analyzed the effects of beam shielding on rainfall retrieval at C band in relatively flat topographical conditions where the main beam blockage source was represented by urban obstacles.

The present work is aimed at evaluating the potential benefit of using polarimetric techniques for operational precipitation retrieval in mountainous areas. In particular, this study is focused on the use of specific differential phase (K_{dp}), it being immune to partial beam shielding and attenuation.

For such purpose, the data coming from two C-band polarimetric radar systems, operating within the Italian radar network, are analyzed. Ten days of observations, for a total of 240 hours, were analyzed. In particular, this work is finalized to: i) clutter removal through the synergy of clutter map, radial velocity and polarimetric texture analysis; ii) partial beam blocking correction; iii) correction of two-way path attenuation; iv) reconstruction of vertical profile of reflectivity; v) differential phase processing and vi) polarimetric estimate of near-surface rainfall.

Several techniques, including a new efficient algorithm for the estimation of specific differential phase, are evaluated. The accomplished analysis outlines encouraging results that might open new scenarios for operational applications. Indeed, rainfall algorithms using specific differential phase resulted to mostly outperform the examined reflectivity-based retrieval techniques.

* *Corresponding author address:* Gianfranco Vulpiani, Department of Civil Protection, Presidency of the Council of Ministers, Rome, Italy;
email: gianfranco.vulpiani@protezionecivile.it

2. DATA SET DESCRIPTION

The radar systems used in the present work belong to the Italian network which provides a coverage of most of the Italian territory with update every 15 min and ground spatial resolution lower than 1 km. The primary justification for a weather radar network in Italy, as well as for other countries, is the detection and warning of severe weather and related hydrogeological risks. The hydrological risk is further enhanced by the topography, which is in Italy characterized by small catchments along most coastlines and by the Alpine and Apennine chains.

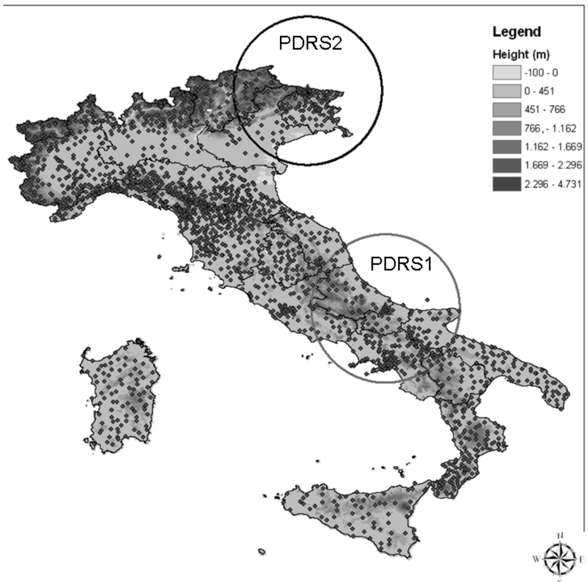

Figure 1 Digital elevation model at 240m horizontal resolution illustrating the complex orography surrounding the considered PDRSs. Circle lines show the nominal radar coverage (i.e., 175 km), raingauges position is represented by dot symbols.

The Polarimetric Doppler Radar Systems (PDRS), located at Mt. Il Monte (hereinafter PDRS1) and Mt. Zoufplan (hereinafter PDRS2), respectively, are two of the six polarimetric radars managed by the Department of Civil Protection. PDRS1 and PDRS2 are respectively located near the border between the Molise and Abruzzo region and Friuli Venezia Giulia region close to Austria, as shown in Figure 1. The Italian radar network siting resulted from the compromise between the radar network fulfilling needs and logistics and environmental requirements. The PDRS1 location, about 700 m above the sea level (A.S.L.), is surrounded in north-western side by the highest peak (about 3000 m) of the Apennine mountain range (see Figure 1); however the Maiella mountain (the higher peak is of about 2800 m) at distance of about 35 km causes the main beam blocking toward the inland country. In such circumstances the major error sources in radar rainfall estimation are obviously related to ground clutter contamination, partial and/or total beam shielding and vertical variability of reflectivity. The PDRS2 site (at about 2000 m altitude) has been chosen to observe the Friuli Venezia Giulia and Veneto valleys characterized by the presence of several catchments (e.g., Tagliamento, Livenza, Isonzo) that are almost fully visible even at low antenna elevation scans.

The considered PDRSs operate at 5.6 GHz with a maximum unambiguous range of about 175 km and range resolution of 0.15 km. The antenna rotation speed has been selected at 12 deg s^{-1}, allowing an integration of 68 samples within the resolution volume.

Seven precipitation events for a total of ten days of observations have been analyzed in the present study. Most of the considered events occurred between spring and autumn, while the two-days event observed by PDRS1 at the beginning of March 2011 was a typical winter Mediterranean storm. Indeed, the euro-atlantic synoptic configuration favoured cold polar fluxes into the Mediterranean area where a deep cut-off low was acting. Specifically, the centre of Italy was affected by a cold front with freezing layer height varying between 1 and 1.5 km A.S.L..

The three-days weather event occurred at the beginning of May 2010 (observed by PDRS2) was the most interesting in terms of persistence and severity. It was characterized by a deep low pressure area (i.e., geopotential height of about 5442-5460 m at 500 hPa) on the centre-western Mediterranean area. At the beginning of the event the Italian territory was affected by a warm conveyor belt transporting wet warm fluxes coming from the African continent. The crucial phase of the storm happened on the 4th May with the beginning of the cyclogenesis on the Gulf of Lion (between France and Spain, close to Marseille. The blocking structure caused the persistence of precipitation with convective phenomena in centre-north Italy, especially on the Alps and northern Apennine areas. The maximum 72-hours cumulated rainfall was about 270mm with maximum daily cumulation of about 153mm on the 4th of May 2010.

X_j	w	$X_{1,j}$	$X_{2,j}$	$X_{3,j}$	$X_{4,j}$
CMAP	0.5	10	30	70	∞
V	0.3	-0.2	-0.1	0.1	0.2
TxZdr	0.4	0.7	1.0	∞	∞
TxRho	0.4	0.1	0.15	∞	∞
TxPhi	0.4	15	20	∞	∞

Table 1. Parameters of the applied system for artefacts removal.

3. DATA PROCESSING

This section describes the radar data processing chain applied to the observed precipitation events. As depicted in Fig. 2, the processing begins with the identification and compensation of non-meteorological echoes and partial beam blockage effects. Secondly, K_{dp} is derived from the filtered Φ_{dp} and used in the rain path attenuation correction module, where external data (i.e., temperature soundings) are also ingested. The mean Vertical Profile of Reflectivity (VPR) is then retrieved and applied to the considered reflectivity-based radar products (i.e., the Lowest Beam Map (LBM) and Vertical Maximum Intensity (VMI)) before computing the rainfall rate. The latter being also estimated through the retrieved specific differential phase.

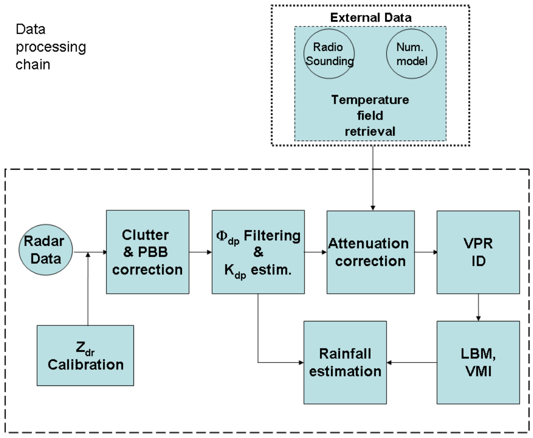

Figure 2 Block Diagram schematically describing the applied radar data processing chain.

3.1 ARTEFACTS REMOVAL, PARTIAL BEAM SHIELDING CORRECTION

The major error sources in radar rainfall estimation are obviously related to ground clutter contamination, partial and/or total beam shielding (especially for PDRS1) and altitude of measurement above ground (i.e., vertical variability of reflectivity).

The radar echoes generated by non-meteorological targets are discriminated from weather returns by means of a quality map Q subjectively generated by combining the following quality indicators: static clutter map (CMAP), radial velocity (V), texture of Z_{dr} (TxZdr), ρ_{hv} (TxRho) and Φ_{dp} (TxPhi). CMAP is a volumetric map obtained by averaging a wide set of reflectivity data observed in clear-air conditions.

For each quality indicator X_j (i.e.,X_1 = CMAP, X_2 = V , X_3 = TxZdr, X_4 = TxRho, X_5 = TxPhi) the degree of membership to the non-meteorological target class d_j is defined through a trapezoidal transformation function

$$d_i = \begin{cases} 0 & \text{if } X_j < X_{1,j} \text{ or } X_j > X_{4,j} \\ \left(X_j - X_{1,j}\right)/\left(X_{2,j} - X_{1,j}\right) & \text{if } X_{1,j} < X_j < X_{2,j} \\ \left(X_{4,j} - X_j\right)/\left(X_{4,j} - X_{3,j}\right) & \text{if } X_{3,j} < X_j < X_{4,j} \\ 1 & \text{if } X_{2,j} < X_j < X_{3,j} \end{cases} \quad (1)$$

where $X_{i,j}$ is the *i-th* vertex of the trapezoid relatively to the *j-th* quality indicator. Table 1 shows the parameterization used for defining d_j. The relative quality index q_j associated to X_j is then defined as the complementary of d_j (i.e., q_j = 1− d_j). Lastly, the overall quality Q is obtained through a weighted sum of the relative quality indices:

$$Q = \sum_j w_j \ q_j \Big/ \sum_j w_j \quad (2)$$

Radar returns with associated low quality (i.e., Q < 0.5) are finally rejected.

An Electromagnetic Propagation Model (EPM) is used to identify the obstructed radial directions. The partial beam blockage (PBB) map, representing the occultation degree at a specific antenna elevation, has been retrieved by resorting to the simplified obstruction function proposed by Bech et al. (2003), assuming the wave propagation in the standard atmosphere (Doviak and Zrnić 1993). The estimated PBB is then compensated up to 70% as in Tabary (2007).

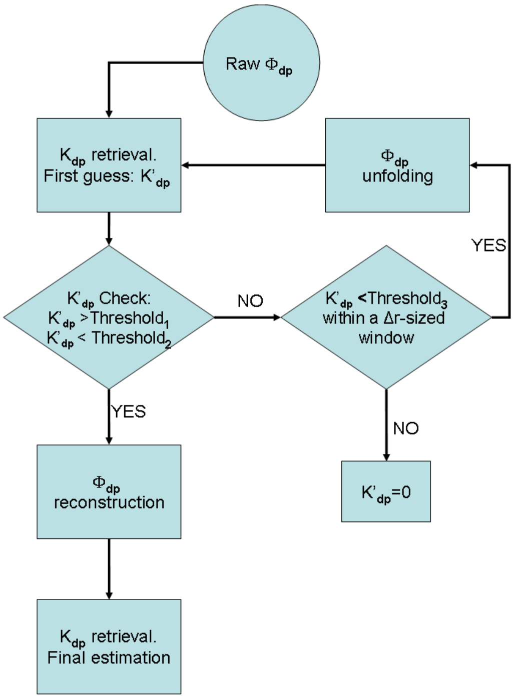

Figure 3 Block diagram describing the applied procedure for Φ_{dp} filtering and K_{dp} retrieval. Regarding the K_{dp} check, it has been assumed that Thresholds$_{1,2,3}$ are −2, 20 and −20 deg km^{-1}, respectively.

3.2 DIFFERENTIAL PHASE PROCESSING

The measured differential phase Ψ_{dp} is the sum of the differential propagation (Φ_{dp}) and backscatter phase (δ_{hv}). However, we are only interested on the propagation component for attenuation correction and rainfall estimation purposes, K_{dp} being related to the range derivative of Φ_{dp}. At C-band frequencies δ_{hv} might not be negligible when resonance scattering occurs. Furthermore, Ψ_{dp} is also conditioned by system noise, offset and potential aliasing problems.

In the present work a multi-step moving-window range derivative approach is applied. As described in Figure 3, the applied methodology can be summarized in four main steps:

i. **K_{dp} retrieval (first guess)**. A first guess of the specific differential phase (K'_{dp}) is retrieved from Ψ_{dp} through a finite-difference scheme over a given sized moving window of length L = 7 km;

ii. **K_{dp} check**. A special care is taken to treat the K_{dp} values that are not manifestly physical, K_{dp} typically ranging between −2 deg km^{-1} (as for vertically oriented ice crystals) and 20 deg km^{-1} (as for heavy rain) at C band (Bringi and Chandrasekar 2001);

iii. **Φ_{dp} reconstruction**. The filtered differential phase is estimated as $\Phi_{dp} = 2\int K'_{dp}(s)\ ds$;

iv. **K_{dp} retrieval (final guess).** The final estimation of the specific differential phase K_{dp} is then obtained as range derivative of the reconstructed Φ_{dp}.

Regarding step ii., we attempt to discriminate anomalously K_{dp} values coming from aliasing or other phenomena (i.e., noise, backscatter differential phase, non-uniform beam filling, residual artefacts). While for the latter cases the estimated K_{dp} are set to zero, in case of Ψ_{dp} wrapping it is necessary to refine the retrieval process. When aliasing occurs, Ψ_{dp} is exposed to a folding of the same order of magnitude of the maximum unambiguous phase shift $\Psi_{dp,max}$ (i.e., 360 degrees for simultaneous transmission). Consequently, the estimated K'_{dp} values would be systematically low (i.e., $K'_{dp} \approx -0.5\cdot 360/L \approx -25$ deg km^{-1}, with L = 7 km) in any L-sized range segment centred at range r_a where aliasing shows up. Once any of such range segments is identified, Ψ_{dp} is unwrapped by adding $\Psi_{dp,max}$ and the whole processing procedure is repeated from $r_a - L/2$ to the end of the range profile. It is interesting to note that following the steps i. – iv. the retrieved differential phase is not affected by the system offset, it being removed when computing K'_{dp}.

According to the uncertainty propagation theory, it can be easily found that the standard deviation of the final K_{dp} becomes

$$\sigma(K_{dp}) = \frac{1}{\sqrt{2N}} \frac{\sigma(\Psi_{dp})}{L} \tag{3}$$

where N is the number of range gates contained in the L-sized moving window (i.e., $N = L/\Delta r$, Δr being the range resolution). This means that for L = 7 km, Δr = 150m and assuming $\sigma(\Psi_{dp})$ = 3 deg, $\sigma(K_{dp})$ is about 0.05 deg km^{-1}.
It is also easy to verify that the standard deviation of the specific differential phase might be further reduced by iterating steps iii. and iv.

$$\sigma\left(K_{dp}{}^{(I)}\right) = \frac{1}{\sqrt{2N^I}} \frac{\sigma(\Psi_{dp})}{L} \tag{4}$$

where I is the number of iterations (with $I \geq 1$).
Consequently, for a lower window size and/or a poorer range resolution Δr (i.e., lower N) it might be possible to get about the same standard deviation by just iterating the retrieval procedure a few times (e.g., $\sigma(K_{dp}) \approx 0.04$ deg km^{-1} for L = 4 km and Δr = 300m with I = 2, assuming $\sigma(\Psi_{dp})$ = 3 deg).

3.3 ATTENUATION CORRECTION

Rain path attenuation is accounted for by applying a slightly different version of the Adaptive PhiDP method (APDP) proposed by

Vulpiani et al. (2008). In order to avoid potential contamination from frozen particles, a fully hydrometeor classification algorithm, adapted from Marzano et al. (2007) by also including the correlation coefficient as input, has been embedded within the adaptive optimization procedure.

The overall new version of the APDP correction procedure can be summarized through the following few steps:

i. the radar observables are filtered from non-meteorological targets and the phase measurements are processed as described in Section 3.1-3.2;

ii. a preliminary attenuation correction is performed assuming a linear relationship between specific co-polar attenuation α_{hh} (as well as specific differential attenuation α_{dp}) and specific differential phase $\alpha_{hh,dp} = \gamma_{hh,dp} K_{dp}$ with fixed values for $\gamma_{hh,dp}$ (i.e., 0.08 and 0.02 deg km^{-1}). At this stage the temperature profile (T), retrieved from the closest available radio sounding, is used to roughly discriminate rain from frozen particles;

iii. the corrected $Z_{hh,dr}$ are then used with K_{dp}, ρ_{hv} and T for a fully hydrometeor classification;

iv. values of $\gamma_{hh,dp}$ are associated to each rain type (i.e., light, moderate, heavy, large drops) as derived from scattering simulations (Vulpiani et al. 2008);

v. at each range distance *r* an optimal $\gamma^{opt}_{hh,dp}(r)$ is computed as the weighted average of the retrieved path-distributed $\gamma_{hh,dp}$, i.e., $\gamma^{opt}_{hh,dp}(r) = \int_0^r K_{dp}(s)\ \gamma_{hh,dp}(s) ds \Big/ \int_0^r \gamma_{hh,dp}(s) ds$

vi. $Z_{hh,dr}$ are finally corrected as

$$Z_{hh,dr}(r) = Z^m_{hh,dr}(r) + 2\int_0^r \gamma^{opt}_{hh,dp}(s)\ K_{dp}(s)\ ds \qquad (5)$$

where $Z^m_{hh,dr}$ represents the measured reflectivity and differential reflectivity, respectively.

3.4 PRECIPITATION ESTIMATION

Once reflectivity is corrected for attenuation, a mean VPR (Joss and Lee 1995) is retrieved from every volume scan (provided that it contains meteorological echoes at all defined height levels) and then applied either to the Lowest Beam Map (LBM) or to the Vertical Maximum Intensity (VMI) in order to get ground-projected reflectivity products. However, we have also considered non-projected reflectivity fields as reference radar products. A standard Z-R relationship (Marshall and Palmer 1948) is applied to reflectivity products. Regarding the K_{dp}-based rain rate algorithm we have considered a general expression of the form $R = a\,|K_{dp}|^b\,sign(K_{dp})$ as suggested by Ryzhkov et al. (2005a). Despite this formula provides unrealistic negative rain rates for negative K_{dp} values, it is adopted in order to compensate the noise effects on the retrieved K_{dp} (i.e., slightly positive and negative rain rates tend to cancel each other when computing the cumulated rainfall). Considering the power-law parameters *a* and *b* derived by either Bringi and Chandrasekar (2001) or Scarchilli et al. (1993) the tested algorithms, denoted as R_{BC} and R_{SC}, respectively, are

$$R_{BC} = 129\ \left(|K_{dp}|/f\right)^{0.85} sign(K_{dp}) \qquad (6)$$

$$R_{SC} = 19.8\ |K_{dp}|\, sign(K_{dp}) \qquad (7)$$

where *f* is the radar frequency expressed in GHz. Relationships (6) and (7) have been applied to the Lowest Beam Map of K_{dp} (LBMK).

The following notation is used to identify the considered algorithms:

- R(LBM(Z)) for rainfall rate computed from LBM;
- R(LBM$_{VPR}$) for rainfall rate computed from ground-projected LBM (through the mean VPR);
- R(VMI(Z)) for rainfall rate computed from VMI;
- R(VMI$_{VPR}$) for rainfall rate computed from ground-projected VMI (through the mean VPR);
- R_{BC}(LBMK) for rainfall rate computed from LBMK using (6);
- R_{SC}(LBMK) for rainfall rate computed from LBMK using (7).

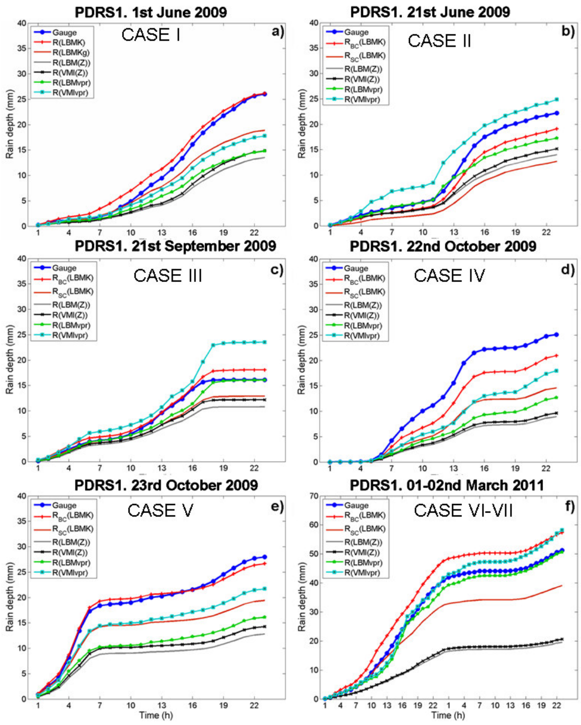

Figure 4 Spatial average of the cumulated rainfall for all the considered algorithms relatively to the storm events observed by PDRS1.

4. RESULTS

This section first describes a qualitative performance analysis, then a quantitative statistical evaluation of the hourly-cumulated precipitation is discussed in terms of the following error indicators:

• Mean Error, $\bar{\varepsilon} = \langle \varepsilon \rangle = \langle R_R - R_G \rangle$;

• Error Standard Deviation, $\sigma_\varepsilon = \sqrt{\langle (\varepsilon - \bar{\varepsilon})^2 \rangle}$;

• Root Mean Square Error, $RMSE = \sqrt{\langle \varepsilon^2 \rangle} = \sqrt{\bar{\varepsilon}^2 + \sigma_\varepsilon{}^2}$;

• Mean Bias, defined as the mean ratio between gauge observation (R_G) and radar estimate (R_R), i.e. $Bias = R_G/R_R$;

Figures 4 and 5 show the spatial average of the cumulated rainfall as a function of time for all the considered algorithms relatively to the storm events observed by PDRS1 and PDRS2, respectively. These figures indirectly provide information on the mean error as a function of the accumulation time. Except for the events VI-VII, depicted on panel f) of Figure 4, it can be noticed that R_{BC} generally outperforms R_{SC} and all the methodologies employing reflectivity when compared to reference gauges (blue curves in Figures 4 and 5). As long as the cumulated precipitation does not exceed 5 – 10mm, R(LBM$_{VPR}$) generally provides a relatively good estimation, i.e. cases II and III, respectively shown in Figure 4 b)-c), are emblematic. Instead, both the considered K_{dp}-based rainfall algorithms depart from the observed rain depths more than R(VMI$_{VPR}$) and R(LBM$_{VPR}$) for the analyzed winter event (No. VI-VII). Indeed, $R_{BC,SC}$(LMBK) are likely conditioned by frozen hydrometeors while the reflectivity-based techniques, especially R(LBM$_{VPR}$), take benefit from the ground projection.

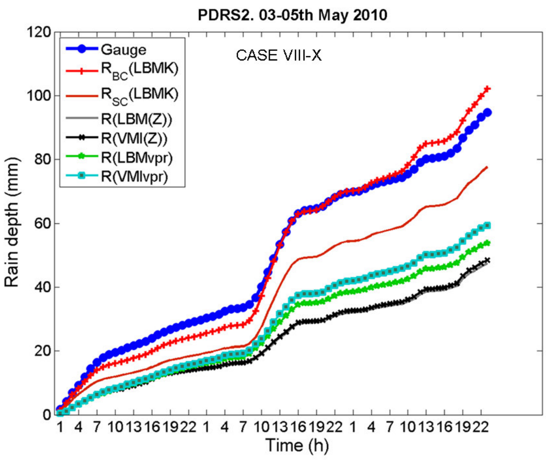

Figure 5 Same as in Figure 4 but relatively to the events observed by PDSR2.

As it can be noticed by Fig. 5, R_{BC}(LBMK) provides, on average, the best performance for the events observed by PDRS2, while R_{SC}(LBMK) and especially the reflectivity-based techniques clearly underestimate precipitation.

Figure 6 shows the spatial distribution of the mean Bias computed on the hourly-cumulated rainfall maps for test cases I, VI-VII and VIII-X relatively to R(VMI(Z)), R(VMI$_{VPR}$), R(LBM$_{VPR}$) and R_{BC}(LBMK).

Generally speaking, R_{BC}(LBMK) provides relatively uniform Bias fields with a tendency to underestimate precipitation in the shielded sector mainly at far ranges due to the likely contamination by frozen particles.

Regarding the considered winter event (1-2nd March 2011), it can also be noticed that R_{BC}(LBMK) slightly overestimates precipitation in the visible sector, in agreement with the findings shown in Figure 4. However, close-range underestimation is also evident in the same case. It might be attributed to disturbance on the measured differential phase caused by side-lobes contamination of low-intensity precipitation observations.

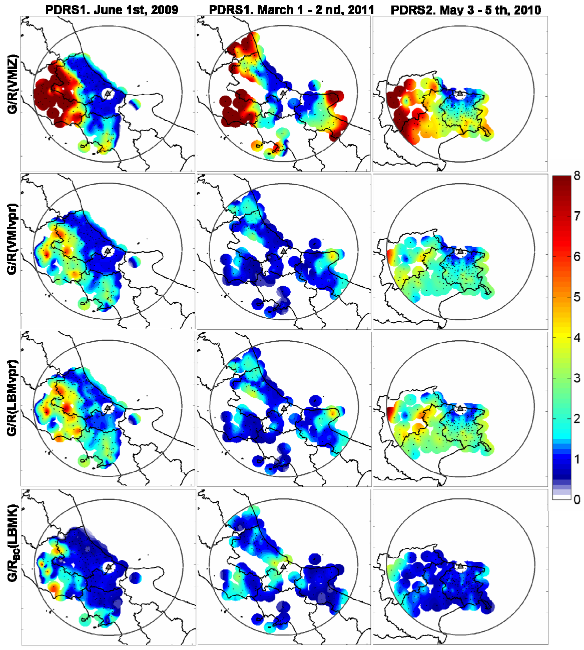

Figure 6 Spatial distribution of the estimated bias for R(VMI), R(VMI$_{VPR}$), R(LBM$_{VPR}$) and R_{BC}(LBMK) relatively to the events No. I, VI-VII and VIII-X.

	R(VMI$_{VPR}$)				R_{BC}(LBMK)			
Case No.	$\bar{\varepsilon}$	σ_ε	*RMSE*	*Bias*	$\bar{\varepsilon}$	σ_ε	*RMSE*	*Bias*
I	-0.59	1.86	1.95	2.09	0.01	1.30	1.30	0.96
II	0.09	3.12	3.12	1.13	-0.15	1.90	1.91	1.16
III	0.10	1.77	1.78	0.99	0.04	1.14	1.41	0.83
IV	-0.54	2.43	2.49	2.37	-0.22	1.80	1.82	1.25
V	-0.37	1.35	1.40	1.50	-0.06	1.17	1.17	1.23
VI-VII	-0.08	2.30	2.30	1.34	-0.09	1.59	1.59	1.15
VIII	-0.69	1.58	1.72	2.97	-0.24	1.19	1.22	1.25
IX	-0.77	1.62	1.79	2.08	0.29	1.36	1.39	0.94
X	-0.42	1.18	1.25	1.60	0.31	1.02	1.07	0.78
VIII-X	-0.61	1.47	1.59	2.14	0.09	1.20	1.21	1.04

Table 2 Overall scores computed on hourly cumulated rainfall.

As it can be seen from Figure 6, the R(VMI(Z)) algorithm generally underestimates rainfall in the blocked sectors where VMI(Z) is constructed from higher elevation scans that might cause precipitation overshooting and/or contamination by ice particles. However, the VMI(Z) ground projection through the application of the mean VPR enables to mitigate these effects. The improvement determined by the VPR correction is outstanding for all the considered events especially for the analyzed winter storm relatively to R(LBM$_{VPR}$). Moreover, the VPR correction causes an average overestimation on the VMI-based rainfall algorithm for Cases II and III, as shown in panels b) and c) of Figure 4.

The overall results are quantitatively confirmed through the considered error statistics summarized in Table 2 for $R(VMI_{VPR})$ and $R_{BC}(LBMK)$. Except for cases I, IV and V, the performance of $R(VMI_{VPR})$ with respect to $R_{BC}(LBMK)$ is characterized by a comparable mean error and mean Bias. However, it is unmistakable that $R_{BC}(LBMK)$ outperforms $R(VMI_{VPR})$ in terms of RMSE by virtue of a lower error standard deviation.

This behaviour, that is particularly evident for the events II, IV and VI-VII, might be attributed to the ground-projection by means of the mean profile of reflectivity, unable (by construction) to catch the VPR spatial variability. Interestingly, $R_{BC}(LBMK)$ produces a mean Bias very close to the optimal value for the test cases I and V with relatively small deviations from unity for the remaining events. Besides, it is important to outline that $R_{BC}(LBMK)$ seems to work efficiently even for a moderate storm such as that observed on the 23rd October 2009 (case V).

CONCLUSIONS

The potential benefit derived by the use of polarimetric methodologies for operational precipitation estimation in complex orography scenarios has been investigated. A couple of dual-polarized C-band radars (named PDRS1 and PDRS2, respectively) belonging to the Italian radar network, respectively sited in central and northern Italy, have been considered togheter with a dense gauge network.

Most of error sources affecting operational radar rainfall estimation have been handled. A combination of clutter map, radial velocity and polarimetric texture analysis is applied for the evaluation of data quality in order to suppress non-meteorological echoes (i.e., ground clutter, clear air echoes, W-LAN interferences). Partial beam blocking effects are accounted for by resorting to an electromagnetic propagation model based on a 240-m digital elevation model.

A new efficient algorithm for differential phase measurements processing and specific differential phase estimation is applied. Rain path attenuation effects are also handled through the adptive use of differential phase measurements. Rain rates fields are finally retrieved either from reflectivity-based radar products (LBM, VMI), eventually ground-projected through the estimate of the mean profile of reflectivity, or by the specific differential phase.

The comparative analysis among Z_{hh}- and K_{dp}-based rainfall algorithms, accomplished on five single-day, one two-days and one three-days events, has shown promising and valuable outcomes from the use of K_{dp} for operational precipitation estimation in presence of complex environmental scenarios. Rainfall fields estimated from the lowest beam map of specific differential phase has generally better marched rain gauges observations, especially in the shielded areas. It is worth mentioning that these results are also confirmed for low-to-moderate rain rates in all considered cases. This may suggest that a K_{dp}-based algorithm may be even applied without resorting to a decision tree where Z_{hh}-based algorithms are employed for less intense rainfall (with the open problem to decide the geographically- and storm-dependent threshold values).

However, this work has outlined the sensitivity of the considered K_{dp}-based rainfall estimators to the presence of dry or melting ice particles. Consequently, future works will be devoted to analyze the sensitivity of polarimetric radar observables on precipitation regime and seasonal dependency in order to set up a rain retrieval technique that could adaptively be used for operational purposes.

REFERENCES

Bech, J., B. Codina, J. Lorente, and D. Bebbington, 2003: The sensitivity of single polarization weather radar beam blockage correction to variability in the vertical refractivity gradient. J. Atmos. Oceanic Technol., 20, 845–855.

Bringi, V. N., V. Chandrasekar, Polarimetric Doppler Weather Radar, 2001. Cambridge, U.K.: Cambridge Univ. Press., pp 636.

Doviak, R. J. and D. S. Zrni´c, 1993: Doppler Radar and Weather Observations. Academic Press. Cambridge University Press, 562 pp.

Friedrich, K., U. Germann, and P. Tabary, 2009: Influence of ground clutter contamination on polarimetric radar parameters. J. Atmos. Oceanic Technol., 26, 251–269.

Giangrande, S. E. and A. V. Ryzhkov, 2008: Estimation of rainfall based on the results of polarimetric echo classification. J. Appl. Meteor. Climatol., 47, 2445-2462.

Joss, J. and R. Lee, 1995: The application of radar-gauge comparisons to operational precipitation profile corrections. J. Appl. Meteorol., 34, 2612–2630.

Marzano, F. S., D. Scaranari, and G. Vulpiani, 2007: Supervised fuzzy-logic classification of hydrometeors using c-band weather radars. IEEE Trans. Geosci. Rem. Sens., 45, 3784–3799.

Ryzhkov, A.V., S.E. Giangrande, and T.J. Schuur, 2005a: Rainfall estimation with a polarimetric prototype of WSR-88D. J. Appl. Meteorol., 44, 502–515.

Ryzhkov, A.V., T.J. Schuur, D.W. Burgess, P.L. Heinselman, S.E. Giangrande, and D.S. Zrnić, 2005b The Joint Polarization Experiment: Polarimetric Rainfall Measurements and Hydrometeor Classification. Bull. Amer. Meteor. Soc., 86, 809–824.

Tabary, P., 2007: The new french operational radar rainfall product. part I: methodology. Wea. Forecasting, 22, 393–408.

Vivekanandan, J., D. N. Yates, and E. A. Brandes, 1999: The influence of terrain on rainfall estimation from reflectivity and specific propagation phase observations. J. Atmos. Oceanic Technol., 16, 837–845.

Vulpiani, G., P. Tabary, J. P. D. Chatelet, and F. S. Marzano, 2008: Comparison of advanced radar polarimetric techniques for operational attenuation correction at c band. J. Atmos.Oceanic Technol., 25, 1118–1135.

Vulpiani, G., S. Giangrande, and F. S. Marzano, 2009: Rainfall estimation from polarimetric S-band radar measurements: Validation of a neural network approach. J. Applied Meteor. Climat., 48, 2022–2036.